Terahertz Quantitative Nondestructive Evaluation of Failure Modes in Polymer-Coated Steel

Junliang Dong, A. Locquet, D. S Citrin

Terahertz Quantitative Nondestructive Evaluation of Failure Modes in Polymer-Coated Steel

Junliang Dong, *Student Member, IEEE,* Alexandre Locquet, D. S. Citrin, *Senior Member, IEEE*

***Abstract*—Terahertz reflective imaging is applied to characterize the failure modes in a polymer coating on a steel plate. The coating was initially scratched, then after accelerated aging, several types of failure have occurred. In order to resolve the thin coating ($\sim$50 μm), terahertz frequency-wavelet domain deconvolution is implemented. With the deconvolved signals, the temporally overlapping echoes of the incident, roughly single-cycle terahertz pulse are clearly resolved, and three important failure modes, *viz.* corrosion, delamination, and blistering, are characterized quantitatively. Terahertz images in three dimensions clearly exhibit the coating thickness distribution across the entire damaged coating, highlighting the terahertz features associated with different failure modes, thus demonstrating that terahertz imaging can be considered as an effective modality for characterizing damage mechanisms in polymer coatings on metals.**

***Index Terms*—Terahertz radiation, Imaging, Protective coatings, Deconvolution, Nondestructive testing**

I. Introduction

NONDESTRUCTIVE evaluation (NDE) techniques for monitoring and characterizing coatings on metals are essential to verify protection of the metal substrate from corrosion during service. Coating failure can have many causes and manifestations. Especially, when a region of a coating system becomes detached from its substrate, the term "adhesion failure" is commonly used. Delamination and blistering are two important types of coating failure in which compromised adhesion is strongly implicated [1]. Since the exact cause and nature of coating failure is still in dispute [2], various NDE techniques have been explored to study damage mechanisms in coatings, such as electrochemical impedance spectroscopy (EIS) [3], scanning electrochemical microscopy [4], acoustic emission [5], and thermography [6][7], to name a few. However, not all of the NDE techniques mentioned above can provide *quantitative* information in depth, nor may they all be capable of monitoring the condition of adhesion. Scanning acoustic microscopy (SAM) [2][8][9] and laser-ultrasonics [10] can provide depth-specific information with enough resolution for characterizing coating systems; however, high attenuation in polymer materials limits the penetration depth of the ultrasonic waves [8]. Therefore, alternative NDE techniques with relatively high resolution are still sought for quantitative evaluation of polymer coatings.

J. Dong, A. Locquet, and D. S. Citrin are with the School of Electrical and Computer Engineering, Georgia Institute of Technology, Atlanta, GA, 30332-0250 USA, and also with UMI 2958 Georgia Tech-CNRS, Georgia Tech Lorraine, 2 Rue Marconi, 57070 Metz, France (e-mail: junliang.dong@gatech.edu; alexandre@gatech.edu; david.citrin@ece.gatech.edu).

Manuscript received XXXX XX, 2016; revised XXXX XX, 2016.

Terahertz (THz) imaging, as a relatively new and promising NDE technique, has attracted considerable interest as a non-invasive, noncontact, and nonionizing method to characterize various non-metallic materials. The THz portion of the electromagnetic spectrum extends from approximately 100 GHz to 10 THz, and lies between the microwaves and infrared; the wavelength range in this region is 3 mm down to 30 μm. THz-frequency electromagnetic waves are known to penetrate numerous nonmetallic materials that may be opaque in the range of visible and infrared light. Moreover, as nonionizing radiation, THz waves present minimal known health risks. Due to these remarkable properties, THz waves have already been successfully used for characterizing materials with multi-layered structures, such as fiber-reinforced composite laminates [11][12], coated pharmaceutical tablets [13][14], dental tissues [15], and art paintings [16]. The application of THz imaging to metals, however, is problematic, as the conductivities of metals preclude significant penetration of the THz radiation below the surface. As a result, metals are typically highly reflective in the THz-frequency range. This reflectivity can be turned to advantage in the NDE of coatings on metals. To date, THz imaging has been demonstrated on automobile paints [17] and marine paints [18], thermal barrier coatings of gas turbine blade [19], and marine protective coatings [20]. Various efforts have also been made to enhance the depth resolution of THz imaging, for example using the time-domain numerical parameter fitting method based on multiple regression analysis [21], fitting the theoretical model with the experiment transfer function in the frequency domain [22], and multivariate analysis [23].

In this study, THz reflective imaging is employed to characterize different failure modes in a one-layered polymer coating on a steel plate. The coating was initially scratched, then after accelerated corrosion over a few months, various types of failure, such as corrosion, delamination, and blistering, are observed to have occurred. Because the thickness of this coating is optically thin in the THz regime, multiple THz echoes partially or totally overlap in the time-domain waveforms, which are particularly noticeable due to the high reflectivity of the metallic substrate. THz frequency-wavelet domain deconvolution is implemented to resolve the overlapping echoes and distinguish the features of various failure modes, especially for revealing the features associated with adhesion failure. Based on the THz deconvolved signals, several failure modes are characterized quantitatively in three dimensions, and the surface topology is successfully reconstructed. Our work thus supports effort to apply THz imaging to investigate the damage mechanisms in polymer coatings on metals.

II. Principle

For samples with layered structure, time-domain THz imaging can provide information in depth by analyzing the reflected THz signals with an incident approximately single-cycle THz pulse. Due to dielectric variations with depth, reflected temporal THz echoes associated with the Fresnel coefficients between various layers are recorded as a function of transverse position in amplitude and time delay. The echo amplitudes provide information on the various refractive indices, while the time delays between THz echoes provide the optical thickness of successive layers. With a knowledge of the refractive indices of the corresponding materials, the physical layer thickness can be extracted. When the layer thickness is optically thin, THz echoes will partially or totally overlap; therefore, the amplitude and time delay cannot be directly extracted from the time-domain waveform. In this case, THz deconvolution can be utilized to resolve the overlapping echoes and reconstruct the intrinsic impulse-response function, and hence the physical structure of the sample studied.

In the time domain, the THz reflected signal (electric field) $r(t)$ is the convolution of the incident THz pulse $i(t)$ with the impulse-response function $h(t)$, which corresponds to the structure and properties of the sample at a given two-dimensional position,

$$r(t) = i(t) \otimes h(t). \tag{1}$$

Deconvolution retrieves the impulse response function $h(t)$ by applying the inverse Fourier transform based on the convolution theorem,

$$h(t) = FFT^{-1}\left[\frac{FFT\big(r(t)\big)}{FFT\big(i(t)\big)}\right], \tag{2}$$

where FFT denotes the Fourier transform and FFT^{-1} the inverse Fourier transform. Frequently, successful deconvolution cannot be expected by directly applying Eq. (2), since division by small numbers will give rise to large spikes in the reconstructed impulse-response function, especially in the high frequency region, leading to severe ringing in the time domain. Therefore, deconvolution process is usually further augmented by frequency-domain filtering to suppress the high-frequency noise, which can be expressed as,

$$h'(t) = FFT^{-1}\left[FFT\big(f(t)\big) \times \frac{FFT\big(r(t)\big)}{FFT\big(i(t)\big)}\right], \tag{3}$$

with $f(t)$ the filter function in the time domain. In order to obtain a successful reconstruction, the temporal duration of $f(t)$ should be short enough to resolve the time intervals between featured echoes, and $f(t)$ should not contain extra signal cycles before or after the main peak, which will obscure the real featured echoes in the reconstructed signal; however, the selection of $f(t)$ is also a compromise between time resolution and frequency-domain filtering [24]. If the duration of $f(t)$ is too short, its frequency spectrum will include large spikes at high frequencies, which will degrade the reconstructed signal in the time domain.

A double Gaussian filter or Wiener filtering can be selected to serve as the frequency-domain filtering [25], and a tapered cosine apodisation function has also been found to work well [26]. Considering the complexity and effectiveness, a Hanning window function is chosen as the filter function $f(t)$ in this study, and its frequency spectrum $F(\omega)$ can be expressed as

$$F(\omega) = \begin{cases} e^{i\omega t_0}\cos^2\left(\frac{\omega}{4f_c}\right) & |\,\omega\,| \leq 2\pi f_c, \\ 0 & |\,\omega\,| > 2\pi f_c, \end{cases} \tag{4}$$

where t_o corresponds to the arrival time of the main peak in the time domain and f_c is the cutoff frequency. This frequency-domain filtering is easy to manipulate just by changing the cutoff frequency f_c. An example of $f(t)$ and its frequency spectrum $F(\omega)$ for typical parameters ($t_0 = 10$ ps and $f_c = 4$ THz) is shown in Fig. 1.

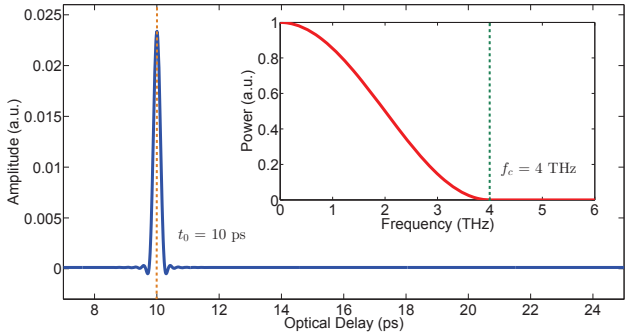

Fig. 1. Hanning window function with typical values, t_0=10 ps and f_c=4 THz, in the time domain and its Fourier transform (power spectrum) in the inset.

Quite often, deconvolution only with frequency-domain filtering cannot guarantee a satisfactory signal-to-noise ratio when a relatively high value of f_c is selected. Stationary wavelet shrinkage is applied to further attenuate the residual noise. This technique decomposes a 1D signal into the approximation coefficients vector and detail coefficients by convolving with a low-pass filter and a high-pass filter along the temporal axis at each level. Wavelet coefficients with small absolute values can be considered as noise, and wavelet coefficients with large absolute values are regarded as the main featured information of the signal [25][27]. Removing the small absolute-value coefficients by thresholding and then reconstructing the signal is expected to produce a signal in which the contribution of noise has been reduced. Sometimes, the signal after frequency-wavelet deconvolution contains slow fluctuations corresponding to the low frequency noise due to the THz source being deficient in the low THz frequency region. This kind of low-frequency noise can be canceled by subtracting the baseline of the deconvolved signal.

III. Experiment

The THz time-domain reflection imaging system (Teraview TPS Spectra 3000), which is employed in this study, is shown schematically in Fig. 2. The GaAs photoconductive antenna is excited by an ultrafast (femtosecond) laser to produce roughly single-cycle THz pulses with bandwidth extending from 60 GHz to 3 THz. The ultrafast laser used here is an Er-doped fiber laser that emits 780 nm pulses with sub-100 femtosecond

This article has been accepted for publication in a future issue of this journal, but has not been fully edited. Content may change prior to final publication. Citation information: DOI 10.1109/JSTQE.2016.2611592, IEEE Journal of Selected Topics in Quantum Electronics

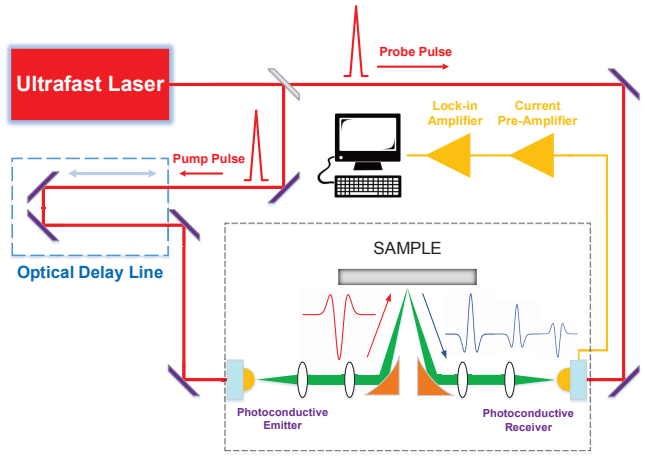

Fig. 2. Schematic diagram of THz time-domain reflection imaging system.

optical pulse duration at a repetition rate of 100 MHz and has an average output power in excess of 65 mW. Coherent detection of the THz radiation is performed in a similar photoconductive antenna circuit. By gating the photoconductive gap with a femtosecond pulse synchronized to the THz emission, a current proportional to the THz electric field is measured. By varying the optical path length, the THz time domain signal can be sampled, resulting in both amplitude and phase information on a sub-picosecond timescale.

In this study, THz imaging is performed in reflection at almost normal incidence. Before imaging the sample, a THz reference signal, shown in Fig. 3, was recorded by setting a bare metal plate (i.e., an excellent THz reflector) at the sample position. The tested sample, shown in Fig. 4(a), is a one-layered polymer (polyester) coating on a zinc-coated steel substrate. Prior to the application of the polymer coating, a thin ($\sim$5 μm) proprietary primer coating was applied. Both the primer and polymer were roll coated onto the substrate. The coating was initially scratched through the coating in the center, and after a multi-month accelerated-corrosion exposure, various types of failure, including corrosion, delamination, and blistering, are visually evident in the coating. Optical microscopy was employed to estimate the thickness of the coating, shown in Fig. 4(b). (The primer coating was not evident in the optical micrographs.) The thickness of the

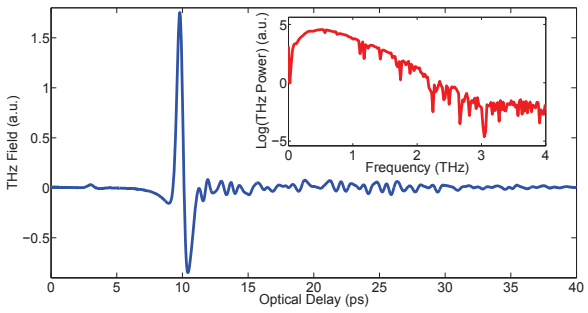

Fig. 3. THz reference signal with its frequency spectrum in the inset.

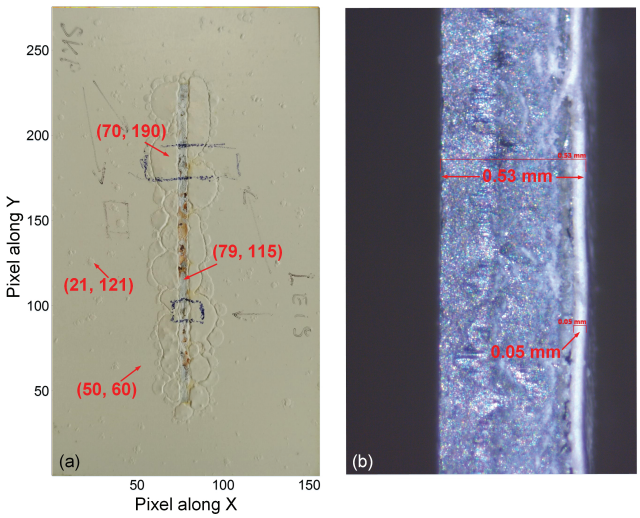

Fig. 4. (a) Visible photograph of the surface of the coating sample with four typical positions highlighted to represent different failure modes. This photograph is also labeled with the pixel number which is the same as the THz C-scans in the following section. (b) Optical micrograph from the edge of the coated sample to roughly estimate the thicknesses of the coating and the steel plate.

coating is about 0.05 mm based on observation from the edge of the sample. We then proceeded with the THz imaging. This sample was raster-scanned by a set of motorized stages moving in x and y directions in 0.2 mm steps over a 33 mm $\times$ 55 mm region of the sample plane, corresponding to 165 $\times$ 275 pixels. Each recorded reflected temporal THz waveform contains 4096 data points, and the signal is averaged over 10 shots per pixel. After completing the scanning, a 3D volume raw data set was acquired.

IV. Results and Discussion

Based on the observation of the coating surface features, four typical positions, which exemplify different failure modes, are selected in Fig. 4(a). The received THz signal at position (50, 60), where no evidently visible damages exist, is shown in Fig. 5(a1). Overlapping THz echoes at this pixel are observed due to the optically thin coating. In order to resolve the overlapping echoes and reveal the structure, THz frequency-wavelet domain deconvolution introduced previously is applied to the raw reflected THz signal at each pixel. In order to make the time resolution as high as possible, the cutoff frequency f_c chosen for all the waveforms is 4 THz. In the wavelet denoising procedure, the *symlet* (sym4) wavelets are selected with a maximum level of 7 for the wavelet decomposition, as no significant improvement can be achieved for higher levels to justify the extra computational expense. After deconvolution, a 3D deconvolved data set is obtained. Peak detection is performed on the deconvolved signals for identifying the existence of an echo. A threshold value for peak detection is set for all pixels, above which we consider a feature as a valid peak.

The deconvolved THz signal at position (50, 60) is shown in Fig. 5(a2). Two positive peaks and one negative peak are clearly identified, which are illustrated in Fig. 5(a3).

This article has been accepted for publication in a future issue of this journal, but has not been fully edited. Content may change prior to final publication. Citation information: DOI 10.1109/JSTQE.2016.2611592, IEEE Journal of Selected Topics in Quantum Electronics

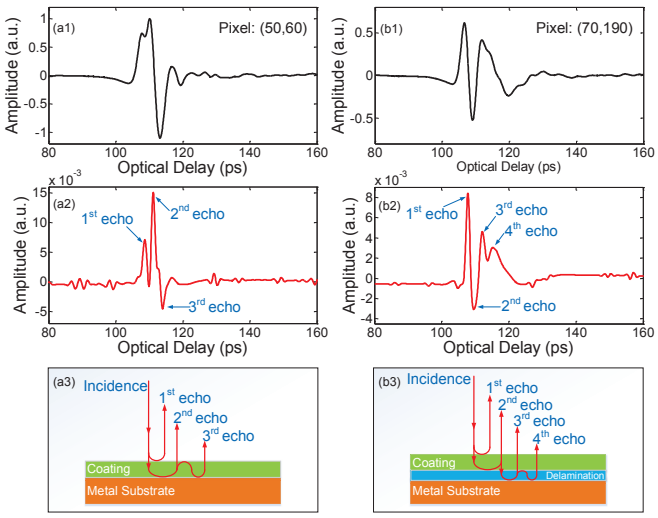

Fig. 5. The THz raw signals [(a1) and (b1)] and deconvolved signals [(a2) and (b2)] at positions (50, 60) and (70, 190), with the corresponding representations of round-trip echoes in [(a3) and (b3)].

The first two positive peaks correspond to the echoes from the air/coating interface and the coating/substrate interface respectively. The third peak, corresponding to the second round echo, is negative due to the phase shift at the coating/air interface. We consider pixels with this kind of deconvolved signal as normal *i.e.*, undamaged, since no features related with damages can be identified. The optical thickness of the coating can be acquired by calculating the optical delay between the first and the second peaks, which is ∼0.5 ps. The refractive index of polyester in the THz range is ∼1.7 [28], therefore, the physical thickness of the coating is ∼44 μm, which is close to the value we estimated with the optical micrograph in Fig. 4(b).

The THz raw signal and deconvolved signal at position (70, 190) are shown in Fig. 5(b1) and (b2). Compared with the normal THz deconvolved signal in Fig. 5(a2), three positive peaks and one negative peak are identified. In this case, the second peak is negative, which indicates the separation between the coating and the substrate, corresponding to the existence of delamination (air gap). The round trip of the identified echoes are illustrated in Fig. 5(b3). Compared with the raw THz signal at this pixel, the deconvolved THz signal clearly reveals the prominent feature associated with the delamination, which is the most important type of adhesive failure. Moreover, the severity of delamination can be evaluated by calculating its physical thickness. With the knowledge of refractive index of air and the measurement of the optical delay between the first peak (positive) and the second peak (negative), the delamination can be characterized quantitatively.

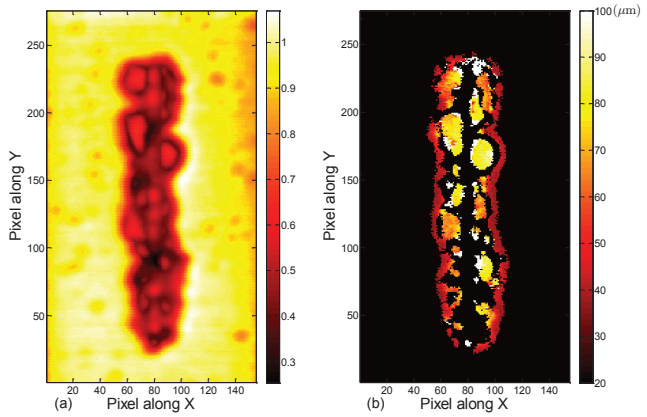

Fig. 6. (a) THz C-scan based on the raw signals with the contrast mechanism as the maximum amplitude of the received signal, which is similar to the optical photograph in Fig. 4(a); (b) THz C-scan based on the deconvolved signals associated with the delamination, which indicates the regions with delamination and the physical thicknesses of the delamination across the coating plane.

THz C-scans can be plotted to provide a two dimensional presentation of data as a top or planar view of features in the coating system. The THz C-scan based on the THz raw data with contrast mechanism as the maximum amplitude value is firstly plotted in Fig. 6(a), which is similar to the optical photograph in Fig. 4(a). Based on the expected features in the deconvolved signal associated with delamination, we can extract all the pixels with this feature present and calculate the physical thickness of the delamination as a function of position. The THz C-scan in Fig. 6(b) clearly exhibits the delamination areas where the existence of air gap is indicated by the THz deconvolved signals. We also obtain the physical thickness of the delamination across the coating plane, which demonstrates that the delamination has been successfully characterized in three dimensions quantitatively by THz imaging.

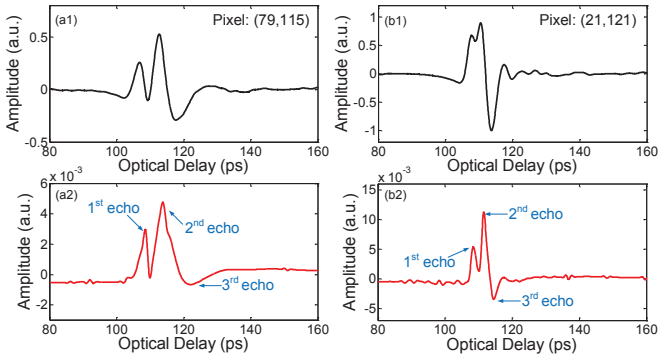

Fig. 7. THz raw signals [(a1) and (b1)] with the corresponding deconvolved signals [(a2) and (b2)] at positions (79, 115) and (21, 121) where a blister is visually present.

The THz raw signal and deconvolved signal at position (79, 115), where the scratch was initially located and the metal oxide first developed upon aging, are shown in Fig. 7(a1) and (a2). The amplitude of the raw and deconvolved signals are relatively small because of the diffuse reflection at the rough surface of the corrosion area. In addition, compared with the signals at the undamaged area, a larger time delay between the first and the second echoes can be observed both in the raw and deconvolved signals. The optical delay in this case corresponds to the thickness of the grown metal oxide due to corrosion at the scratch area.

Next, we discuss the signal features at the blisters. The THz

This article has been accepted for publication in a future issue of this journal, but has not been fully edited. Content may change prior to final publication. Citation information: DOI 10.1109/JSTQE.2016.2611592, IEEE Journal of Selected Topics in Quantum Electronics

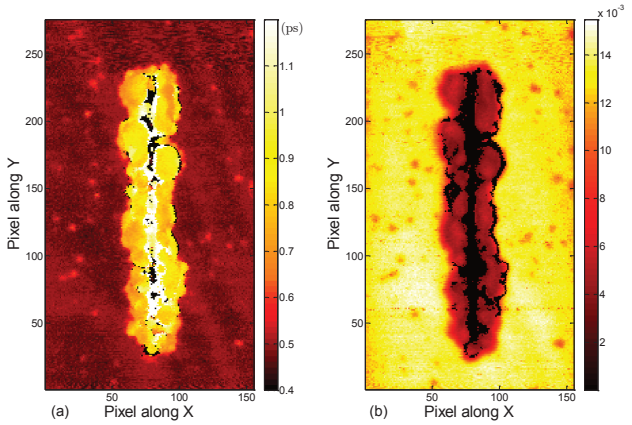

Fig. 8. (a) THz C-scan based on the optical delay between the first positive peak and second positive peak in the deconvolved signals, which represents the optical distance between the coating surface and the top surface of the metal substrate; (b) THz C-scan based on the amplitude of the second positive peak in the deconvolved signals, which indicates the adhesive condition.

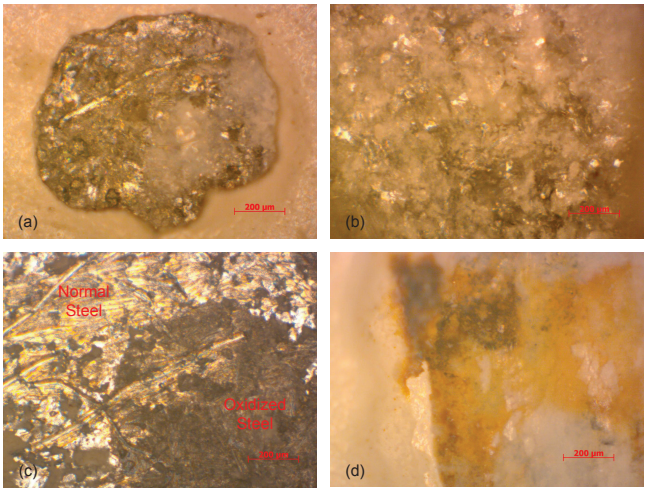

Fig. 9. Optical micrographs associated with different failure modes after peeling off the coating. (a) Oxidized substrate in the blistering area; (b) Oxidized substrate in the delamination area; (c) Comparison between the steel substrate at the undamaged area and the blistering area by peeling off the coating at one blister area and the adjacent undamaged area; (d) Grown metal oxide due to corrosion along the scratch.

raw signal and deconvolved signal at position (21, 121), where a blister is clearly observed, are shown in Fig. 7(b1) and (b2). Both THz raw and deconvolved signals present quite similar features compared with the signals at the undamaged area. However, by careful comparison with the THz deconvolved signal at the undamaged area in Fig. 5(a2), we observe: (1) the optical delay between the first and the second echoes is larger in blisters; (2) the amplitude of the second echo is smaller in blisters. Based on these two features, THz C-scans are plotted in Fig. 8 to reveal all the blisters in the coating. In Fig. 8(a), THz C-scan is plotted based on the optical delay between the first two positive peaks of the deconvolved signals, which represents the optical distance between the coating surface and the top surface of the metal substrate. The blistering areas, represented as red spots in the image, are clearly revealed. Compared with the undamaged areas, the blisters are associated with a slightly larger optical thickness, and the delamination and corrosion areas around the scratch exhibit much larger optical distance due to the existence of the air gap under the delaminated coating or the metal oxide, respectively. In Fig. 8(b), THz C-scan is plotted based on the amplitude of the second positive peak, which indicates the condition of adhesion, because the second peak corresponds to the echo bouncing back after reflecting off the substrate. Compared with the undamaged areas, the blisters show smaller amplitude which indicates a weaker adhesion with the substrate, with the delamination areas exhibit much weaker adhesion, *viz.* adhesion failure.

The physical origin of the contrast between blisters and the surrounding undamaged regions are now discussed. Compared with the undamaged area, the relatively large optical delay between the first two positive peaks at the locations of the blisters is due to the separation between the coating and the substrate and the existence of the air gap. However, the air gap under the blisters is too small to be resolved even in the deconvolved signals. In this case, the negative peak corresponding to the echo from the coating/air interface and the positive peak corresponding to the echo from the air/substrate are not well-separated and largely cancel with each other. The result of this overlap and cancellation is only one observable positive peak with a later arrival time and smaller amplitude compared with the peak corresponding to the echo from the coating/substrate interface in undamaged areas [12][29]. Another reason, which is also responsible for the smaller amplitude of the second positive peak, is the presence of oxidization of the metal substrate in blisters locations induced by the accelerated aging. The oxidized substrate under the blisters provides a smaller reflection compared with the normal steel under the undamaged coating, where the coating and the substrate adhere tightly and an almost total reflection can be expected.

Optical microscopy was next employed to verify the physical explanations above. In order to observe the conditions of adhesion associated with different failure modes, the coating at representative positions is carefully removed. Compared with the undamaged areas, the coating at delamination and

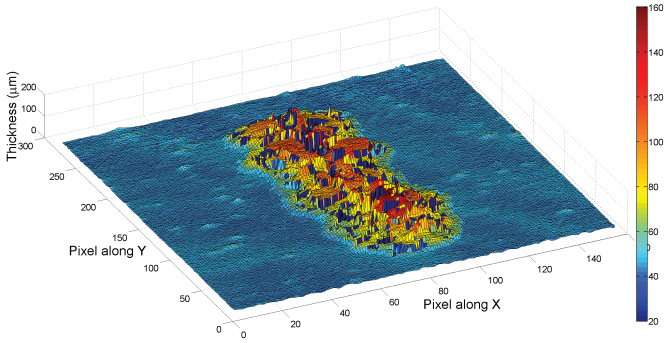

Fig. 10. THz image of the thickness distribution, as well as the surface topology, of the coating. Different failure modes, including corrosion, delamination, and blistering, have been characterized quantitatively in three dimensions.

blistering areas is easier to peel off due to the existence of an air gap. Optical micrographs in areas with blistering, delamination and corrosion along the scratech are shown in Fig. 9(a), (b), (d), respectively. Oxidized substrate is observed under both the blister and delamination. Comparison between the substrate in the undamaged area and under the blister is shown in Fig. 9(c) by peeling off the coating at one blister and the adjacent undamaged area. The substrate in the undamaged area is visually shiny; on the contrary, the oxidized substrate under the blister appears black in the optical micrograph. The optical micrographs support our conclusions above based on the THz images concerning the compromised adhesion of the coating in these areas.

Based on the analysis above, the characteristics of various failure modes, including corrosion, delamination, and blistering, have been successfully revealed using time-domain THz reflective imaging. The thickness distribution of this damaged coating can be estimated, as shown in Fig. 10. To do this, we assume that the refractive indices of the corrosion (metal oxide) is similar to that of the coating [30]. We note in the image the metal oxide is grown in the scratch area, on both sides of which are raised areas of delaminations. Beyond this is a relatively flat area with isolated raised areas due to blisters. With this 3D image, the thicknesses associated with various failure modes, as well as the surface topology of the coating system are clearly reconstructed, exhibiting the capability of THz imaging for the quantitative NDE of polymer coatings on metals.

V. Conclusion

In this study, THz reflective imaging was demonstrated to characterize different failure modes in a polyester-coated zinc-coated steel plate. THz frequency-wavelet domain deconvolution was adapted to resolve the optically thin coating. Based on the deconvolved signals, the characteristics of various failure modes, including corrosion, delamination, and blistering, have been successfully identified. The THz deconvolved signals also enable us to evaluate the condition of adhesion, especially for the delamination and blisters, which are related with adhesion failure. The thickness distribution across the entire damaged coating, as well as its surface topology is also obtained. These interpretations were supported by optical microscopy. Based on these results, we conclude that THz imaging, which can provide a noninvasive, noncontact, and nonionizing modality for characterizing coatings quantitatively in three dimensions, can be utilized as an effective tool for investigating the damage mechanisms and monitoring the corrosion process in polymer-coated metals.

Acknowledgment

The authors gratefully acknowledge the financial support of the Conseil Régional de Lorraine and the Fonds Européen de Développement Régional (FEDER). The authors thank Sophie Berveiller and Denis Bouscaud for their help in the analysis of the samples.

References

[1] J. Graystone and R. Kennedy, "Non-destructive measurement of coating adhesion," *Surface Coatings International*, vol. 83, no. 8, pp. 389–398, 2000.

[2] I. A. Koch, M. Bargmann, H. Oehler, D. Lellinger, M. Wanner, and D, "Investigation of delamination mechanisms in polymer coatings by scanning acoustic microscopy," *Journal of Physics D: Applied Physics*, vol. 44, no. 3, p. 34009, 2011.

[3] K. Darowicki, P. Ślepski, and M. Szociński, "Application of the dynamic EIS to investigation of transport within organic coatings," *Progress in Organic Coatings*, vol. 52, no. 4, pp. 306–310, 2005.

[4] R. M. Souto, Y. González-García, J. Izquierdo, and S. González, "Examination of organic coatings on metallic substrates by scanning electrochemical microscopy in feedback mode: Revealing the early stages of coating breakdown in corrosive environments," *Corrosion Science*, vol. 52, no. 3, pp. 748–753, 2010.

[5] A. Gallego, J. F. Gil, E. Castro, and R. Piotrkowski, "Identification of coating damage processes in corroded galvanized steel by acoustic emission wavelet analysis," *Surface and Coatings Technology*, vol. 201, no. 8, pp. 4743–4756, 2007.

[6] Y. He, G. Y. Tian, M. Pan, D. Chen, and H. Zhang, "An investigation into eddy current pulsed thermography for detection of corrosion blister," *Corrosion Science*, vol. 78, pp. 1–6, 2014.

[7] A. Schönberger, S. Virtanen, V. Giese, C. Spießberger, H. Schröttner, J. Rattenberger, and J. Wagner, "Non-destructive evaluation of stone-impact damages using pulsed phase thermography," *Corrosion Science*, vol. 56, pp. 168–175, 2012.

[8] I. Alig, S. Tadjbach, P. Krüger, H. Oehler, and D. Lellinger, "Characterization of coating systems by scanning acoustic microscopy: Debonding, blistering and surface topology," *Progress in Organic Coatings*, vol. 64, no. 23, pp. 112–119, 2009.

[9] H. Oehler, I. Alig, D. Lellinger, and M. Bargmann, "Failure modes in organic coatings studied by scanning acoustic microscopy," *Progress in Organic Coatings*, vol. 74, no. 4, pp. 719–725, 2012.

[10] Y. Watanabe, S. Fujisawa, A. Yonezu, and X. Chen, "Quantitative evaluation of adhesion quality of surface coating by using pulse laser-induced ultrasonic waves," *Surface and Coatings Technology*, vol. 286, pp. 231–238, 2016.

[11] J. Dong, B. Kim, A. Locquet, P. McKeon, N. Declercq, and D. S. Citrin, "Nondestructive evaluation of forced delamination in glass fiber-reinforced composites by terahertz and ultrasonic waves," *Composites Part B: Engineering*, vol. 79, no. 0, pp. 667–675, 2015.

[12] J. Dong, A. Locquet, N. F. Declercq, and D. S. Citrin, "Polarization-resolved terahertz imaging of intra- and inter-laminar damages in hybrid fiber-reinforced composite laminate subject to low-velocity impact," *Composites Part B: Engineering*, vol. 92, pp. 167–174, 2016.

[13] Y. C. Shen and P. F. Taday, "Development and application of terahertz pulsed imaging for nondestructive inspection of pharmaceutical tablet," *Selected Topics in Quantum Electronics, IEEE Journal of*, vol. 14, no. 2, pp. 407–415, 2008.

[14] H. Lin, Y. Dong, Y. C. Shen, and J. Axel Zeitler, "Quantifying pharmaceutical film coating with optical coherence tomography and terahertz pulsed imaging: An evaluation," *Journal of Pharmaceutical Sciences*, vol. 104, no. 10, pp. 3377–3385, jun 2016.

[15] D. Crawley, C. Longbottom, V. P. Wallace, B. Cole, D. Arnone, and M. Pepper, "Three-dimensional terahertz pulse imaging of dental tissue," *Journal of Biomedical Optics*, vol. 8, no. 2, pp. 303–307, 2003.

[16] M. Picollo, K. Fukunaga, and J. Labaune, "Obtaining noninvasive stratigraphic details of panel paintings using terahertz time domain spectroscopy imaging system," *Journal of Cultural Heritage*, vol. 16, no. 1, pp. 73–80, 2015.

[17] K. Su, Y. C. Shen, and J. Axel Zeitler, "Terahertz sensor for non-contact thickness and quality measurement of automobile paints of varying complexity," *Terahertz Science and Technology, IEEE Transactions on*, vol. 4, no. 4, pp. 432–439, 2014.

[18] J. Choi, W. S. Kwon, K.-S. Kim, and S. Kim, "Nondestructive evaluation of multilayered paint films in ambient atmosphere using terahertz reflection spectroscopy," *NDT & E International*, vol. 80, pp. 71–76, 2016.

[19] T. Fukuchi, N. Fuse, M. Okada, T. Ozeki, T. Fujii, M. Mizuno, and K. Fukunaga, "Topcoat Thickness Measurement of Thermal Barrier Coating of Gas Turbine Blade Using Terahertz Wave," *Electrical Engineering in Japan*, vol. 189, no. 1, pp. 1–8, 2014.

[20] W. Tu, S. Zhong, Y. C. Shen, and A. Incecik, "Nondestructive testing of marine protective coatings using terahertz waves with stationary wavelet transform," *Ocean Engineering*, vol. 111, pp. 582–592, 2016.

[21] T. Yasuda, T. Iwata, T. Araki, and T. Yasui, "Improvement of minimum paint film thickness for THz paint meters by multiple-regression analysis," *Applied Optics*, vol. 46, no. 30, pp. 7518–7526, 2007.

[22] M. Scheller and M. Koch, "Fast and accurate thickness determination of unknown materials using terahertz time domain spectroscopy," *Journal of Infrared, Millimeter, and Terahertz Waves*, vol. 30, no. 7, pp. 762–769, 2009.

[23] T. Iwata, S. Yoshioka, S. Nakamura, Y. Mizutani, and T. Yasui, "Prediction of the thickness of a thin paint film by applying a modified partial-least-squares-1 method to data obtained in terahertz reflectometry," *Journal of Infrared, Millimeter, and Terahertz Waves*, vol. 34, no. 10, pp. 646–659, 2013.

[24] J. R. Fletcher, G. P. Swift, D. Dai, J. M. Chamberlain, and P. C. Upadhya, "Pulsed terahertz signal reconstruction," *Journal of Applied Physics*, vol. 102, no. 11, p. 113105, 2007.

[25] Y. Chen, S. Huang, and E. Pickwell-MacPherson, "Frequency-wavelet domain deconvolution for terahertz reflection imaging and spectroscopy," *Optics Express*, vol. 18, no. 2, pp. 1177–1190, 2010.

[26] R. K. H. Galvão, S. Hadjiloucas, A. Zafiropoulos, G. C. Walker, J. W. Bowen, and R. Dudley, "Optimization of apodization functions in terahertz transient spectrometry," *Optics Letters*, vol. 32, no. 20, pp. 3008–3010, 2007.

[27] J. Dong, A. Locquet, and D. S. Citrin, "Enhanced Terahertz Imaging of Small Forced Delamination in Woven Glass Fibre-reinforced Composites with Wavelet De-noising," *Journal of Infrared, Millimeter, and Terahertz Waves*, vol. 37, no. 3, pp. 289–301, 2015.

[28] J. Yun-Sik, K. Geun-Ju, and J. Seok-Gy, "Terahertz Dielectric Properties of Polymers," *Journal of Korean Physical Society*, vol. 49, no. 2, p. S. 513, 2006.

[29] M. Schwerdtfeger, E. Castro-Camus, K. Krügener, W. Viöl, and M. Koch, "Beating the wavelength limit: three-dimensional imaging of buried subwavelength fractures in sculpture and construction materials by terahertz time-domain reflection spectroscopy," *Applied Optics*, vol. 52, no. 3, pp. 375–380, 2013.

[30] N. Fuse, T. Fukuchi, T. Takahashi, M. Mizuno, and K. Fukunaga, "Evaluation of applicability of noncontact analysis methods to detect rust regions in coated steel plates," *IEEE Transactions on Terahertz Science and Technology*, vol. 2, no. 2, pp. 242–249, 2012.

Junliang Dong (S'16) received the M.S. degree in control science and engineering from Tsinghua University, China, in 2011. He is currently working toward the Ph.D. degree in Georgia Institute of Technology. His research interests include terahertz imaging and spectroscopy, terahertz optics, and non-destructive testing.

Alexandre Locquet received the M.S. degree in electrical engineering from the Faculté Polytechnique de Mons, Mons, Belgium, the Ph.D. degree (doctorat) in engineering science, and electrical and computer engineering from the Université de Franche-Comté, Besançon, France, and the Ph.D. degree in electrical and computer engineering from the Georgia Institute of Technology (Georgia Tech), Atlanta, GA, USA. He is currently a Researcher with the Unité Mixte Internationale, Georgia Tech-CNRS Laboratory, Georgia Tech Lorraine, Metz, France, and an adjunct professor with the School of Electrical and Computer Engineering, Georgia Tech. His research interests are in semiconductor laser dynamics and chaos, nonlinear time series analysis, physical-layer security, and terahertz imaging. He has authored or co-authored over 40 journal publications and conference presentations, and one book chapter. He is a member of Eta Kappa Nu, the Optical Society of America (OSA), and the IEEE Photonics Society.

D. S. Citrin (M'93-SM'03) received the B.A. degree from Williams College, Williamstown, MA, USA, in 1985, and the M.S. and Ph.D. degrees from the University of Illinois Champaign, IL, USA, in 1987 and 1991, respectively, all in Physics. From 1992 to 1993, he was a Post-Doctoral Research Fellow with the Max Planck Institute for Solid State Research, Stuttgart, Germany, where he was involved in exciton radiative decay in low-dimensional semiconductor structures. Subsequently, from 1993 to 1995, he was a Center Fellow with the Center for Ultrafast Optical Science, University of Michigan, Ann Arbor, MI, USA, where he studied ultrafast phenomena in quantum wells. He was then an Assistant Professor of Physics with Washington State University, Pullman, WA, USA from 1995-2001. In 2001, he joined the faculty of the Georgia Institute of Technology, where he is currently a Professor of Electrical and Computer Engineering. In addition, he coordinates the research effort on Nonlinear Optics and Dynamics with the Unité Mixte Internationale, Georgia Tech-CNRS UMI 2958 at Georgia Tech Lorraine, Metz, France. His research interests include terahertz science and technology, nonlinear dynamics in external-cavity semiconductor lasers, and nanophotonics. He has served as an Associate Editor of the IEEE JOURNAL OF QUANTUM ELECTRONICS. He was a recipient of the Presidential Early Career Award for Scientists and Engineers and the Friedrich Bessel Prize from the Alexandre von Humboldt Stiftung.